

# Complete analysis of a transmission electron diffraction pattern of a MoS<sub>2</sub>–graphite heterostructure



Marlene Adrian, Arne Senftleben\*, Silvio Morgenstern, Thomas Baumert

University of Kassel, Institute of Physics and Center for Interdisciplinary Nanostructure Science and Technology (CINaT), Heinrich-Plett-Straße 40, D-34132 Kassel, Germany

## ARTICLE INFO

### Article history:

Received 6 November 2015

Received in revised form

30 March 2016

Accepted 8 April 2016

Available online 9 April 2016

### Keywords:

Electron diffraction

Moiré pattern

Superstructure

Van der Waals heterostructure

## ABSTRACT

The combination of various 2D layered materials in multilayer heterostructures arises great interest in the current science. Due to the large variety of electronic properties of the group of 2D layered materials the combination opens a new pathway towards ultrasmall electronic devices. In this contribution we present a full mathematical description of multilayer heterostructure samples and their diffraction patterns including a proposal of a consistent assignment of the superstructure diffraction spots. A 27 nm thick MoS<sub>2</sub>–graphite heterostructure was produced and fully analysed with the methods presented in this paper.

© 2016 Elsevier B.V. All rights reserved.

## 1. Introduction

Two-dimensional materials consist of covalently joined layers, which are vertically stacked by van der Waals forces. The electronic properties of layered materials vary from pure insulators to metallic conductors and can even be dependent on the number of layers [1]. The combination of different types of bonds within one material leads to remarkable inter- and intra-layer transport properties. The combination of two-dimensional materials in multilayer heterostructures is expected to open up a broad field of application in electronics and sensor technology [2,3]. It is therefore essential to investigate the fundamental properties of such systems.

A matter of particular interest is the formation of a Moiré pattern caused by the superposition of several layered materials. This superstructure appears in diffraction patterns of the heterostructure and contains all information about the interlayer structural properties. A full mathematical description of the superstructure in real space and reciprocal space is presented in Section 2. The corresponding nomenclature for the appearing spots in the diffraction pattern of a free-standing multilayer heterostructure is explained in Section 3. A free-standing sample preparation enables us to study the characteristics of a multilayer van der Waals heterostructure without the influence of any substrate effect. Our preparation procedure follows a proposal by Jannik Meyer [4],

which is based on the exfoliation method by Andre Geim and Konstantin Novoselov [5]. This preparation method is presented in Section 4 and already has proved to be successful in the preparation of free-standing samples of few-layer graphite [6] and molybdenum disulphide.

In general, Ultrafast Electron Diffraction (UED) is a direct approach to study structural dynamics following optical excitation [6–14]. In this contribution we use the experimental UED set-up presented in Section 5 to take static diffraction patterns of a free-standing sample of a molybdenum disulphide–graphite heterostructure. Finally we present a fully characterized free-standing sample of a molybdenum disulphide–graphite heterostructure and a complete assignment of its static diffraction pattern in Section 6.

## 2. Mathematical description of Moiré pattern

In this section we will focus on the discussion of the superstructure symmetry and its mathematical description. The mathematical description of the superstructure is essential for the complete assignment of the diffraction pattern of a van der Waals heterostructure. The combination of two hexagonal two-dimensional materials leads to the formation of a Moiré pattern. The superstructure arises from the superposition of atomic positions in real space, the corresponding diffraction pattern in Fourier space is built by a two-dimensional convolution of the diffraction patterns of the individual materials. This leads to additional superstructure diffraction spots encircling every material Bragg spot. The origin of

\* Corresponding author.

E-mail address: [arne.senftleben@uni-kassel.de](mailto:arne.senftleben@uni-kassel.de) (A. Senftleben).

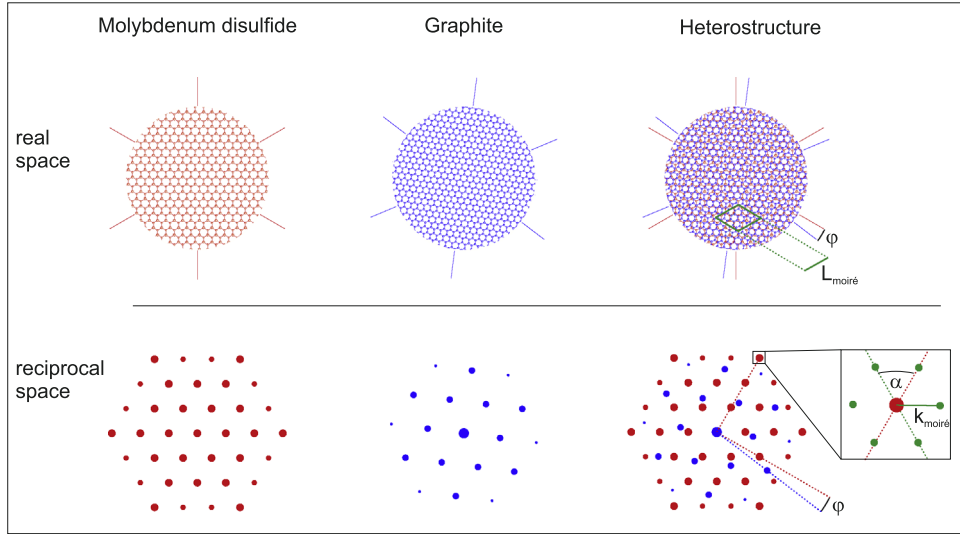


**Fig. 1.** Schematic example of the origin of the superstructure in real space and reciprocal space. The combination of molybdenum disulphide (red) and graphite (blue), which are misaligned by an angle of  $\varphi = -7.3^\circ$ , leads to the formation of a Moiré pattern in real space. The superstructure in real space arises from the superposition of atomic positions, the corresponding diffraction pattern in Fourier space is built by a two-dimensional convolution of the diffraction patterns of the individual materials. This leads to additional superstructure diffraction spots (green) encircling every material Bragg spot. The superstructure is rotated by an angle  $\alpha$  with respect to the lattice orientation of molybdenum disulphide. (For interpretation of the references to color in this figure legend, the reader is referred to the web version of this article.)

the peaks leads to the fact that every superstructure diffraction spot with the same relative orientation to a specific material Bragg spot contains the same information. A schematic example of the formation of a Moiré superstructure and the corresponding diffraction pattern by the combination of molybdenum disulphide and graphite is shown in Fig. 1.

Due to the fact that the materials are stacked along their axis of six-fold rotational symmetry, this six-fold rotational symmetry is preserved in the multilayer heterostructure. The missing periodicity along the  $c$ -axis leads in the case of a combination of two different materials to the space group 6, as in our case, or to 6 mm if the rotational angle between the layers is either  $\varphi = 0^\circ$  or  $\varphi = 30^\circ$  and thus, the presence of  $\sigma_v$  mirror planes is allowed. In both cases we do not observe any symmetry elements that are affecting the coordinate along the  $c$ -axis. Therefore, we will only consider the in-plane contributions when developing a mathematical description for the arising Moiré pattern.

The in-plane real-space lattice coordinates of any hexagonal material can be described by a set of basis vectors  $\vec{a}_1$  and  $\vec{a}_2$  which we choose according to Fig. 2 to be:

$$\begin{aligned} \vec{a}_1 &= \frac{a}{2} \begin{pmatrix} \sqrt{3} \\ -1 \end{pmatrix} \\ \vec{a}_2 &= a \begin{pmatrix} 0 \\ 1 \end{pmatrix} \end{aligned} \quad (1)$$

The angle between the real-space basis vectors is  $120^\circ$  and  $a$  is the real-space lattice constant of the specific material. The corresponding reciprocal lattice vectors are then obtained to be:

$$\begin{aligned} \vec{a}_1^* &= \frac{4\pi}{\sqrt{3}a} \begin{pmatrix} 1 \\ 0 \end{pmatrix} = a^* \begin{pmatrix} 1 \\ 0 \end{pmatrix} \\ \vec{a}_2^* &= \frac{2\pi}{\sqrt{3}a} \begin{pmatrix} 1 \\ \sqrt{3} \end{pmatrix} = \frac{a^*}{2} \begin{pmatrix} 1 \\ \sqrt{3} \end{pmatrix} \end{aligned} \quad (2)$$

with  $a^* = \frac{4\pi}{\sqrt{3}a}$  being the length of the reciprocal lattice vector.

The spatial properties in real space of this lattice (described by a function  $f_a(\vec{r})$ ) can be represented by an infinite Fourier series

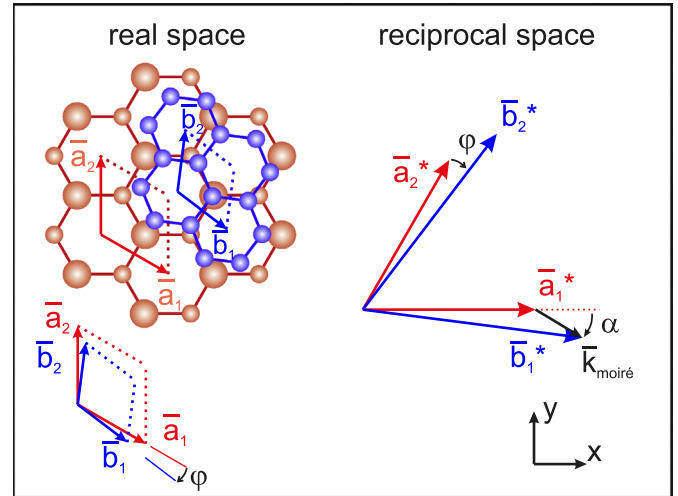


**Fig. 2.** The in-plane real-space lattice coordinates of the hexagonal materials are described by a set of basis vectors  $(\vec{a}_1, \vec{a}_2)$  and  $(\vec{b}_1, \vec{b}_2)$  which we choose to be  $\vec{a}_1 = \frac{a}{2}(\sqrt{3}, -1)$  and  $\vec{a}_2 = a(0, 1)$ . The angle between the real-space basis vectors is  $120^\circ$  and  $a$  is the real-space lattice constant of the first material. The second lattice with lattice constant  $b$  is rotated anticlockwise with respect to lattice  $a$  by an angle of  $\varphi$ . The example is shown for  $\varphi = -7.3^\circ$ . The corresponding lattice vectors are then obtained to be  $\vec{b}_1 = \frac{b}{2}(\sqrt{3} \cos \varphi + \sin \varphi, \sqrt{3} \sin \varphi - \cos \varphi)$  and  $\vec{b}_2 = b(-\sin \varphi, \cos \varphi)$ . The set of reciprocal in-plane lattice vectors  $(\vec{a}_1^*, \vec{a}_2^*)$  and  $(\vec{b}_1^*, \vec{b}_2^*)$  is by definition also rotated anticlockwise by an angle of  $\varphi$ . The first order reciprocal lattice vector of the Moiré pattern  $\vec{k}_{\text{Moiré}}$  is obtained by subtraction of the reciprocal lattice vectors  $\vec{b}_1^* - \vec{a}_1^*$ .

with, in general, complex valued coefficients  $c_{j,k}^a$  [15].

$$f_a(\vec{r}) = \sum_{j,k} \left( c_{j,k}^a \cdot \exp \left( i \left( j \cdot \vec{a}_1^* + k \cdot \vec{a}_2^* \right) \cdot \vec{r} \right) \right) \quad (3)$$

The second lattice with lattice constant  $b$  is rotated anticlockwise with respect to lattice  $a$  by an angle of  $\varphi$ . This leads to the following set of reciprocal lattice vectors for the second lattice.

$$\begin{aligned}\vec{b}_1^* &= b^* \begin{pmatrix} \cos \varphi \\ \sin \varphi \end{pmatrix} \\ \vec{b}_2^* &= \frac{b^*}{2} \begin{pmatrix} \cos \varphi - \sqrt{3} \sin \varphi \\ \sin \varphi + \sqrt{3} \cos \varphi \end{pmatrix} \quad \text{with } b^* = \frac{4\pi}{\sqrt{3}b}\end{aligned}\quad (4)$$

In accordance with (3), the spatial properties in real space of the second lattice  $b$  are described by a function  $f_b(\vec{r})$  which can also be represented by an infinite Fourier series with complex valued coefficients  $c_{j,k}^b$ .

$$f_b(\vec{r}) = \sum_{j,k} \left( c_{j,k}^b \exp \left( i \left( j \cdot \vec{b}_1^* + k \cdot \vec{b}_2^* \right) \cdot \vec{r} \right) \right) \quad (5)$$

We define a lattice mismatch  $\delta$  between the lattice constants of the two lattices involved.

$$\delta = 1 - \frac{b}{a} = 1 - \frac{a^*}{b^*} \quad (6)$$

As a standard we always choose the lattice with the larger real-space lattice constant to be lattice  $a$ , the one with the smaller real-space lattice constant to be lattice  $b$ . That results in  $a \geq b$  or  $a^* \leq b^*$  respectively and  $0 < \delta \leq 1$ . Due to the six-fold rotational symmetry of the van der Waals heterostructure we also restrict  $\varphi$  to  $-30^\circ < \varphi \leq 30^\circ$ .

### 2.1. First order Moiré pattern

As the Moiré superstructure arises from a superposition of two lattices  $a$  and  $b$  in real space, the spatial properties of this superstructure can be described by the following function  $f(\vec{r})$ , which can always be formally represented by an infinite Fourier series with respect to the basis vectors of lattice  $a$  [15]. This Fourier expansion is modulated by factors  $a_{j,k}^M$ , which are periodic.

$$\begin{aligned}f(\vec{r}) &= f_a(\vec{r}) + f_b(\vec{r}) = \sum_{j,k} \left( c_{j,k}^a \exp \left( i \left( j \cdot \vec{a}_1^* + k \cdot \vec{a}_2^* \right) \cdot \vec{r} \right) \cdot a_{j,k}^M(\vec{r}) \right) \\ \text{with } a_{j,k}^M(\vec{r}) &= 1 + \frac{c_{j,k}^b}{c_{j,k}^a} \exp \left( i \left( j \cdot \left( \vec{b}_1^* - \vec{a}_1^* \right) + k \cdot \left( \vec{b}_2^* - \vec{a}_2^* \right) \right) \cdot \vec{r} \right) \quad (7)\end{aligned}$$

First order reciprocal lattice vectors of the Moiré pattern can be obtained from the difference between the respective reciprocal lattice vectors of the materials.

$$\begin{aligned}\vec{k}_{\text{Moiré},1} &= \vec{b}_1^* - \vec{a}_1^* \\ \vec{k}_{\text{Moiré},2} &= \vec{b}_2^* - \vec{a}_2^*\end{aligned}\quad (8)$$

This results in

$$a_{j,k}^M(\vec{r}) = 1 + \frac{c_{j,k}^b}{c_{j,k}^a} \exp \left( i \left( j \cdot \vec{k}_{\text{Moiré},1} + k \cdot \vec{k}_{\text{Moiré},2} \right) \cdot \vec{r} \right) \quad (9)$$

The positions of the Moiré pattern diffraction spots can be fully described by the length of the corresponding reciprocal lattice vector

$$\begin{aligned}\left| \vec{k}_{\text{Moiré}} \right| &= \left| \vec{k}_{\text{Moiré},1} \right| = \left| \vec{k}_{\text{Moiré},2} \right| \\ \left| \vec{k}_{\text{Moiré}} \right| &= \sqrt{a^{*2} + b^{*2} - 2a^*b^* \cos \varphi} \\ &= \frac{a^*}{1-\delta} \sqrt{\delta^2 + 2(1-\delta)(1-\cos \varphi)} \\ &= \frac{4\pi}{\sqrt{3}a(1-\delta)} \sqrt{\delta^2 + 2(1-\delta)(1-\cos \varphi)} \quad (10)\end{aligned}$$

and the angle  $\alpha$  between the reciprocal lattice vector  $\vec{a}_1^*$  and  $\vec{k}_{\text{Moiré}}$ .

$$\tan \alpha = \frac{\sin \varphi}{\cos \varphi - (1-\delta)} \quad (11)$$

### 2.2. Description of all possible Moiré patterns

The description given so far applies for the first order diffraction spots of the Moiré pattern. But in addition higher order diffraction spots of the Moiré superstructure occur in the diffraction pattern of a van der Waals heterostructure. These higher order diffraction spots arise from a correlation of higher order Bragg peaks of the individual materials, i.e. from a linear combination of the basis vectors  $\vec{a}_1^*$  and  $\vec{a}_2^*$  as well as  $\vec{b}_1^*$  and  $\vec{b}_2^*$ .

In this case we describe the reciprocal lattice vectors  $\vec{k}_a$  and  $\vec{k}_b$  of the two materials as a linear combination of their basis vectors.

$$\begin{aligned}\vec{k}_a(m, n) &= m \cdot \vec{a}_1^* + n \cdot \vec{a}_2^* \quad \text{with } \left| \vec{k}_a \right| = a^* \sqrt{m^2 + n^2 + mn} \\ \vec{k}_b(r, s) &= r \cdot \vec{b}_1^* + s \cdot \vec{b}_2^* \quad \text{with } \left| \vec{k}_b \right| = b^* \sqrt{r^2 + s^2 + rs}\end{aligned}\quad (12)$$

In accordance with (7) and (8), the reciprocal lattice vector of the Moiré pattern is calculated by the interaction between the two reciprocal lattice vectors  $\vec{k}_a$  and  $\vec{k}_b$ . Only one reciprocal lattice vector of the superstructure will be considered in the further description, because due to the sixfold symmetry of the Moiré pattern (space group 6), the second reciprocal basis vector can be calculated by a rotation of  $60^\circ$  of the first basis vector.

$$\begin{aligned}\vec{k}_{(mnrs)} &= \vec{k}_b(r, s) - \vec{k}_a(m, n) \\ &= \frac{a^*}{2(1-\delta)} \begin{pmatrix} (2r+s) \cos \varphi - \sqrt{3}s \sin \varphi - (2m+n)(1-\delta) \\ (2r+s) \sin \varphi + \sqrt{3}s \cos \varphi - \sqrt{3}n(1-\delta) \end{pmatrix} \quad (13)\end{aligned}$$

The length of the reciprocal lattice vector of the superstructure is then given by:

$$\begin{aligned}\left| k_{(mnrs)} \right|^2 &= a^{*2}(m^2 + n^2 + mn) + b^{*2}(r^2 + s^2 + rs) \\ &\quad - a^*b^*(m(2r+s) + n(2s+r)) \cos(\varphi) \\ &\quad + \sqrt{3}(nr - ms) \sin(\varphi) \\ &= \left( \frac{a^*}{1-\delta} \right)^2 \left( -(1-\delta)(m(2r+s) + n(r+2s)) \cos \varphi \right. \\ &\quad \left. + \sqrt{3}(1-\delta)(ms - nr) \sin \varphi \right. \\ &\quad \left. + (1-\delta)^2(m^2 + n^2 + mn) + r^2 + s^2 + rs \right) \quad (14)\end{aligned}$$

The real-space lattice constant of the superstructure  $|L_{(mnrs)}|$  can be calculated from the length of the reciprocal lattice vector  $|k_{(mnrs)}|$ .

$$|L_{(mnrs)}| = \frac{4\pi}{\sqrt{3}|k_{(mnrs)}|} \quad (15)$$

In addition, the angle  $\alpha_{(mnrs)}$  between the standard reciprocal lattice vector  $\vec{a}_1^*$  and  $\vec{k}_{(mnrs)}$  can be calculated.

$$\tan(\alpha_{(mnrs)}) = \frac{(2r+s) \sin \varphi + \sqrt{3}s \cos \varphi - \sqrt{3}n(1-\delta)}{(2r+s) \cos \varphi - \sqrt{3}s \sin \varphi - (2m+n)(1-\delta)} \quad (16)$$

The first order description is fully covered by this extended description.

### 3. Labelling of the diffraction spots of a multilayer heterostructure

In this section we will describe how we propose to label the

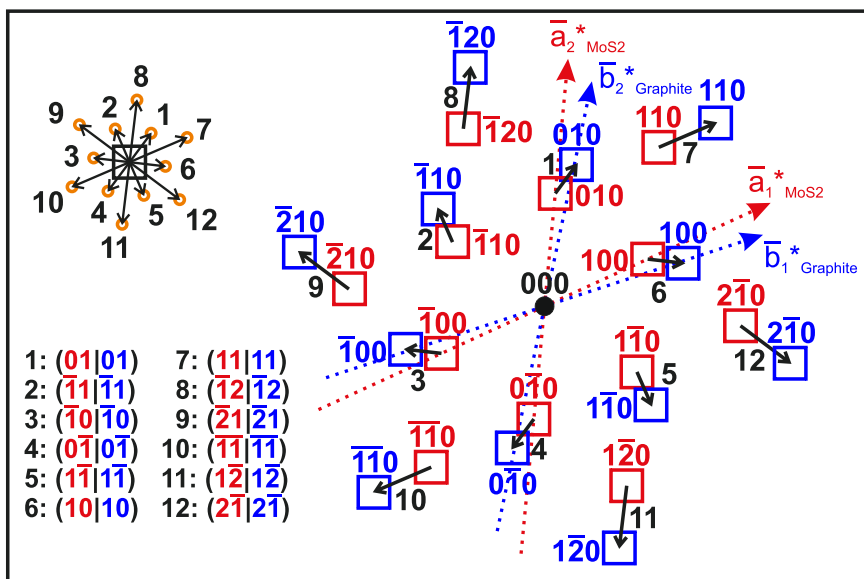


**Fig. 3.** Derivation of the nomenclature of the superstructure diffraction spots. The superstructure diffraction spots which are encircling every material Bragg spot are derived from specific difference between the lattice vectors of the individual materials. The schematic on the left shows the position of the superstructure diffraction peaks (orange circles) in relation to the position of a material Bragg spot (black square). On the right hand side, the corresponding lattice vector difference is plotted. We propose to label the superstructure peaks according to the reciprocal lattice vectors they originate from. These reciprocal lattice vectors can be described as a linear combination of the reciprocal basis vectors, as shown in (12). As a standard we always put the material with the smaller reciprocal lattice constant at first. So, the superstructure diffraction spots are labelled  $(mnr|s)$  with  $m$  and  $n$  being the in-plane scalar factors of the primary material and  $r$  and  $s$  the in-plane scalars of the material with the larger reciprocal lattice constant. As the reciprocal lattice vectors occur as material Bragg spots in the diffraction pattern, the scalars  $m$ ,  $n$ ,  $r$  and  $s$  correspond to the in-plane Miller indices  $h$  and  $k$  of the matching Bragg spots. The labels of the first (No. 1–6) and second order (No. 7–12) superstructure diffraction spots are given in the scheme at the upper left. (For interpretation of the references to color in this figure legend, the reader is referred to the web version of this article.)

diffraction spots in a diffraction pattern of a multilayer heterostructure. Similar to the common Miller index labelling for crystalline Bragg peaks we label the superstructure peaks according to the respective reciprocal lattice vectors that have been derived in the previous section.

As already mentioned we use the convention that lattice  $a$  has the larger real-space lattice constant than lattice  $b$ . Initially, the diffraction spots of the material with larger real-space lattice constant are labelled with the Miller indices  $(hkl)_a$  as in a usual diffraction pattern. In the next step, the basis vectors  $\vec{b}_1^*$  and  $\vec{b}_2^*$  are chosen such that  $-30^\circ \leq \varphi < 30^\circ$  applies. On that basis, the diffraction spots of lattice  $b$  are labelled with the Miller indices  $(hkl)_b$ .

The superstructure diffraction spots are then labelled according to the reciprocal lattice vectors they originate from. These reciprocal lattice vectors can be described as a linear combination of the reciprocal basis vectors, as shown in (12). The length of the superstructure reciprocal lattice vector  $|k_{(mnr|s)}|$  as well as its orientation angle  $\alpha_{(mnr|s)}$  can be described by the scalars  $m$ ,  $n$ ,  $r$  and  $s$  of the linear combination. Therefore, we propose to label the superstructure diffraction spots with  $(mnr|s)$  (see Fig. 3). This labelling method uses the same reference frame, e.g. the same set of basis vectors, for the labelling of both the material Bragg spots as well as the superstructure diffraction spots.

As the superstructure arises from the superposition of atomic positions in real space, the corresponding diffraction pattern in Fourier space is built by a two-dimensional convolution of the diffraction patterns of the individual materials. This leads to the additional superstructure diffraction spots encircling every material Bragg spot. The origin of the peaks leads to the fact that every superstructure diffraction spot with the same relative orientation to a specific material Bragg spot contains the same information. Therefore, the declaration of the corresponding material Bragg spot, a specific superstructure diffraction spot is located at, is not necessary.

#### 4. Preparation and characterization of free-standing single crystalline heterostructures

Our method for the preparation of free-standing multilayer heterostructures follows two different procedures. These procedures are on the one hand based on a method which was primarily realised by Jannik Meyer in 2005 at the University of California in Berkeley [16]. The second procedure is based on a method proposed in 2014 by Andres Castellanos-Gomez [17]. The principle of mechanical exfoliation introduced by Konstantin Novoselov and Andre Geim [5] provides the basis for both procedures.

The method by Jannik Meyer uses semiconductor grade adhesive tape for multiple mechanical exfoliation steps to cleave the layered material. The procedure by Andres Castellanos-Gomez uses transparent viscoelastic stamps made from commercially available gel film instead of adhesive tape for the mechanical exfoliation steps. Already during exfoliation, this method allows the determination of the thickness of a desired sample by measurement of the transmittance. In both methods, the obtained few layers of single crystal flakes are deposited on an oxide coated silicon wafer. Flakes of adequate size are characterized by optical reflection microscopy and atomic force microscopy.

In order to prepare free-standing samples, the flakes have to be transferred onto a Quantifoil TEM gold grid which is covered by an amorphous carbon film. This film is selectively removed from one grid hole via laser machining before the transfer process in order to reduce the background signal in the electron diffraction patterns and to avoid additional substrate effects in the experiments. In addition, the experimental set-up requires samples of about 100  $\mu\text{m}$  diameter. The desired sample flake is transferred onto the grid by an etching process of the silicon dioxide using potassium hydroxide.

The preparation of multilayer heterostructures uses the exfoliation procedure for the materials of interest separately. The

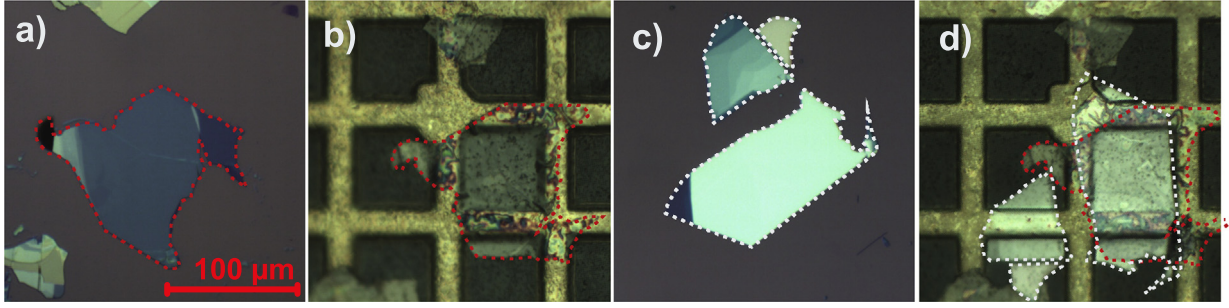


**Fig. 4.** Stepwise process of preparation of a multilayer van der Waals heterostructure. In a first step the graphite sample is transferred to the modified grid. Subsequently the molybdenum disulphide flake is transferred on top of the graphite sample on the grid. The dashed red line indicates the contour of the graphite flake, while the dashed white line shows the shape of the molybdenum disulphide flakes. (For interpretation of the references to color in this figure legend, the reader is referred to the web version of this article.)

multilayer heterostructure is then successively built up by repetition of the transfer process. We prepared a free-standing sample of a molybdenum disulphide-graphite heterostructure by the procedure mentioned above. As it can be seen in Fig. 4 the graphite sample flake was transferred onto the empty modified grid. In a second step a sample flake of molybdenum disulphide was transferred on top of the free-standing graphite sample (see Fig. 4(c) and (d)).

The free-standing samples can be characterized easily by determination of the transmittance of bright white light. The transmittance of the sample is dependent on the thickness of the material layers according to Beer-Lambert's law. Up to ten layers a linear decrease of the transmittance with the number of layers is a good assumption. In case of graphite the absorption of white light per layer is 2.3% [18] while molybdenum disulphide is reported to absorb 5.5% of white light per layer [19]. Measurement of the transmittance of the first material and of the whole heterostructure allows to reliably determine the thickness of both materials.

The transmittance of the prepared free-standing heterostructure sample displayed in Fig. 4 is determined to be 11%. As shown in Fig. 5 the transmittance of the pure free-standing graphite layer is 41%. The transmittance of the pure molybdenum disulphide layer cannot be measured directly due to underlying substrate (either graphite layer or amorphous carbon film) but can be calculated from the transmittance of the pure free-standing graphite layer ( $T_{\text{graphite}} = I_{\text{graphite}}/I_0$ ) and the transmittance of the combined heterostructure ( $T_{\text{hetero}} = I_{\text{hetero}}/I_0$ ) by  $T_{\text{MoS}_2} = I_{\text{hetero}}/I_{\text{graphite}} = T_{\text{hetero}}/T_{\text{graphite}}$ . This allows the determination of the transmittance of the molybdenum disulphide layer to be 28%. This data shows that our free-standing sample of a molybdenum disulphide-graphite van der Waals

heterostructure contains about 38 layers of graphite and about 23 layers of molybdenum disulphide, thus twice as many layers of graphite as of molybdenum disulphide.

The relative scattering intensity can be estimated from the structure factors  $F_{hkl}$  which can be derived from the atomic form factors  $f_i$  of the individual atoms in a unit cell.

$$F_{hkl} = \sum_j^N f_j \cdot \exp(2\pi i(u_{j,1}h + u_{j,2}k + u_{j,3}l)) \quad (17)$$

with  $u_{j,1}$ ,  $u_{j,2}$  and  $u_{j,3}$  being the relative position of all  $N$  atoms labelled  $j$  in the unit cell. This leads to a ratio of

$$\frac{F_{100,C}}{F_{100,\text{MoS}_2}} = \frac{4f_C}{2 \cdot (f_{\text{Mo}} + 2f_S)} \quad (18)$$

This ratio reflects the fact that the graphite unit cell contains four carbon atoms, while the unit cell of molybdenum disulphide contains two formula units of  $\text{MoS}_2$ . The scattering intensity is proportional to  $|F_{hkl}|^2$ .

$$I_{hkl} \propto |F_{hkl}|^2 \quad (19)$$

The atomic form factors ( $f_C = 6.0$  e/atom,  $f_{\text{Mo}} = 42.4$  e/atom,  $f_S = 16.0$  e/atom, energy range 40–60 keV) were taken from [20]. That results in

$$\frac{F_{100,C}}{F_{100,\text{MoS}_2}} \approx 16\% \quad \text{or} \quad \frac{|F_{100,C}|^2}{|F_{100,\text{MoS}_2}|^2} \approx 2.6\% \quad (20)$$

The difference in the scattering intensity complicates the diffraction pattern analysis and could be compensated by an appropriate

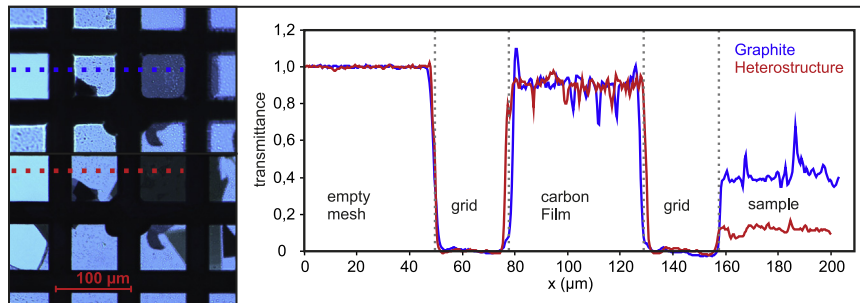


**Fig. 5.** Determination of sample thickness by transmittance analysis. The left panel shows pictures of the pure graphite sample (top) and the multilayer heterostructure sample (bottom) in transmission white light set-up. The transmittance along the dashed lines is plotted in the right panel. The blue colour indicates the graphite sample, the red colour belongs to the heterostructure. The transmittance is a function of sample thickness and can therefore be used to calculate the thickness of the two material layers. The transmittance of the graphite layer was measured to be 41% which indicates 38 layers of graphite. The transmittance of the van der Waals heterostructure was measured to be 11%. Due to the transmittance of graphite the transmittance of the molybdenum disulphide can be determined to be 28%. This value arises from 23 layers of molybdenum disulphide. The van der Waals heterostructure is composed of 38 layers of graphite and 23 layers of molybdenum disulphide. (For interpretation of the references to color in this figure legend, the reader is referred to the web version of this article.)

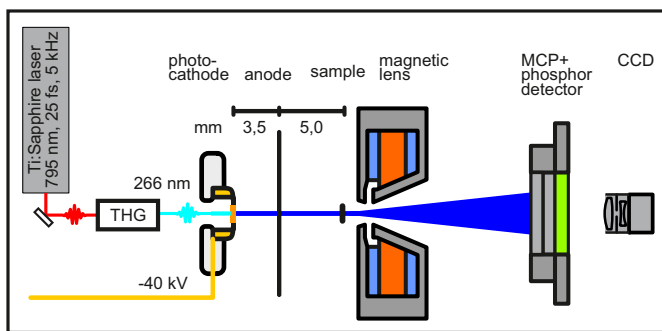


**Fig. 6.** Schematic representation of Electron Diffraction set-up. A 266 nm laser beam is used to generate electrons by emission from a gold photocathode. The electrons are accelerated by a voltage of up to 40 kV in direction of an anode. After passing the anode through a hole of 100  $\mu\text{m}$  diameter the electrons hit the sample placed behind. The scattered electrons are focused by a magnetic lens on the detection unit which uses micro-channel plates (MCP) to enhance the electron signal and a P43 phosphor screen to convert the electron signal into light signals. These light signals are then recorded by a CCD-camera. The number of electrons per pulse is adjusted by control of the UV-pulse energy.

ratio of number of layers of the different materials. But in order to be able to look at possible energy transfer processes inside the heterostructure sample, it is necessary to have a comparable thickness of both materials.

## 5. Experimental set-up

The experimental set-up for transmission electron diffraction is shown in Fig. 6. The current set-up uses a Ti:Sapphire laser amplifier system emitting laser pulses with a central wavelength of

795 nm and a pulse duration of 25 fs at a repetition rate of 5 kHz.

The electron pulses are generated by emission of photoelectrons from a gold photocathode placed inside the vacuum chamber (1 mm sapphire coated with 3 nm Ti-Cr and 40 nm gold). The required UV-pulses which are able to overcome the work function are generated in a frequency conversion unit by successive second harmonic generation and sum frequency generation to produce the third harmonic of the infrared fs laser radiation from the amplifier system (THG = Third harmonic generation). After passing a prism compressor for dispersion compensation the UV-pulses are focused on the photocathode. The generated pulses of photoelectrons are accelerated in direction of an anode by a voltage of up to 40 kV. The electrons pass the anode through a hole of 100  $\mu\text{m}$  diameter and hit the sample placed behind. The scattered electrons are focused by a magnetic lens on the detection unit which uses micro-channel plates (MCP) to enhance the electron signal and a P43 phosphor screen to convert the electron signal into light signals. These light signals are then recorded by a 1 Megapixel CCD-camera at a distance of 188 mm from the electron source. The number of electrons per pulse is adjusted by control of the UV-pulse energy.

## 6. Results

The diffraction pattern obtained from the free-standing sample of a molybdenum disulphide-graphite van der Waals heterostructure is shown in Fig. 7. The sample was oriented in such a way that the electron pulses first pass the molybdenum disulphide layer and afterwards the graphite layer. This means that the graphite layer is facing the detector side. The opposite orientation

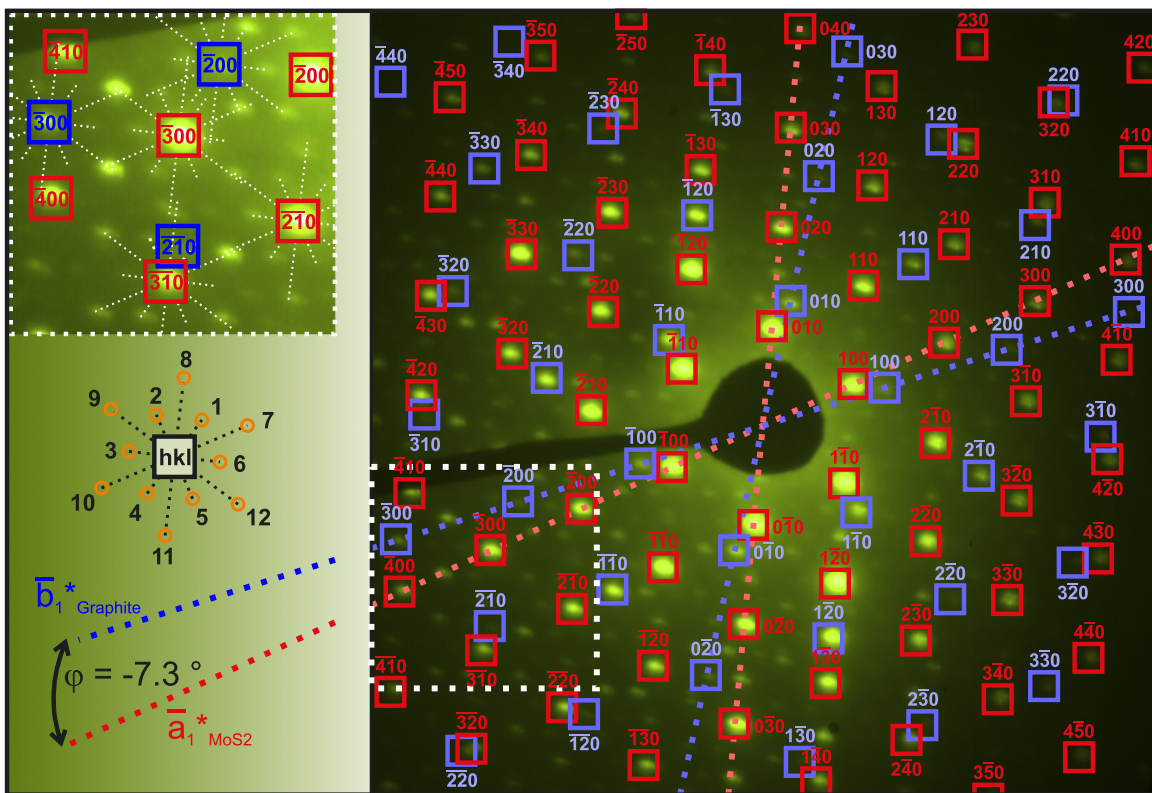


**Fig. 7.** The diffraction pattern of the multilayer van der Waals heterostructure consists of the diffraction patterns of the individual materials and the superstructure. The material diffraction patterns are indicated by the open squares. The red squares correspond to the Bragg peaks of molybdenum disulphide, the blue squares indicate the graphite diffraction peaks. The section displayed by the dashed white line is enlarged on the left of the picture. Here, the twelve visible superstructure diffraction spots encircling every material Bragg spot can be seen. It is also indicated that the angle  $\varphi$  between the material layers can easily be extracted from the diffraction pattern. In this case it is determined to be  $-7.3^\circ$ . (For interpretation of the references to color in this figure legend, the reader is referred to the web version of this article.)

**Table 1**Values of  $|k_{(mnirs)}|$  and  $\alpha_{(mnirs)}$  from the diffraction pattern.

(mnirs)	Measurement		Calculation from (14)–(16)		
	$ k_{(mnirs)} $	$\alpha_{(mnirs)}$	$ k_{(mnirs)} $	$\alpha_{(mnirs)}$	$ L_{(mnirs)} $
(01101)	$0.74 \text{ \AA}^{-1}$	$28.7^\circ$	$0.73 \text{ \AA}^{-1}$	$29.2^\circ$	$9.91 \text{ \AA}$
11111)	$1.28 \text{ \AA}^{-1}$	$-1.3^\circ$	$1.27 \text{ \AA}^{-1}$	$-0.8^\circ$	$5.72 \text{ \AA}$

yields the mirror image of the diffraction pattern. Because molybdenum disulphide possesses the larger real-space lattice constant, it is chosen to be material *a* in this heterostructure. The Bragg spots arising from molybdenum disulphide are plotted and labelled in red, the Bragg spots of graphite in blue. The labelling followed the rules we proposed in Section 3.

The scattering intensity is plotted on a logarithmic scale. The integral intensity of the first order graphite Bragg spots are in the range of 15% to 25% of the integral intensity of the first order Bragg spots of molybdenum disulphide. This shows that although the number of layers of both materials is of the same order of magnitude (see Section 4), the ratio of scattering intensity is sufficient for detailed diffraction pattern analysis.

It can be seen that the graphite layer is rotated by an angle of  $\varphi = -7.3^\circ$  with respect to the molybdenum disulphide. The section displayed by the dashed white line is enlarged on the left of the whole diffraction pattern. In this section, the superstructure diffraction spots which are encircling every material Bragg spot, are clearly visible. The schematic below the enlarged section shows the position of the superstructure diffraction spots with respect to each Bragg spot.

The origin of the twelve visible superstructure diffraction spots is explained in Fig. 3. The superstructure diffraction spots are labelled according to Section 3 and Eq. (14) with (mnirs).

From the diffraction pattern analysis we determined the values of  $|k_{(mnirs)}|$  and  $\alpha_{(mnirs)}$  and compared them to the values obtained from (14) and (16). The values for the superstructure Bragg peaks (01101) and (11111) can be found in Table 1.

The rotational angle of  $\varphi = -7.3^\circ$  with respect to the molybdenum disulphide coincides with the rotational angle in the example in Fig. 1. The superstructure unit cell was calculated with (15) and (16). It can easily be seen that it matches the real-space image quite well.

## 7. Conclusion

In this paper, we presented a full mathematical description of Moiré superstructures in real space and reciprocal space. This description is able to predict all structural parameters of van der Waals heterostructures from the corresponding diffraction pattern. A well working method was used for the preparation of really free-standing multilayer heterostructures. The thickness of the individual material layers was determined by transmission of white light. The resulting diffraction pattern of the heterostructure can be fully described and analysed. On that basis, further measurements of the structural dynamics inside a van der Waals heterostructure following ultrashort laser excitation are possible.

## Acknowledgements

We thank Birk Fritsch for his valued contribution to the preparation of thin exfoliated sample flakes of graphite and molybdenum disulphide on top of oxide coated silicon wafers. Alexander Kastner and Christian Sarpe are gratefully acknowledged for their technical support on the laser system.

## References

- [1] S. Lebègue, T. Bjorkman, M. Klintonberg, R.M. Nieminen, O. Eriksson, Two-dimensional materials from data filtering and ab initio calculations, *Phys. Rev. X* 3 (3) (2013) 31002.
- [2] A.K. Geim, I.V. Grigorieva, Van der waals heterostructures, *Nature* 499 (7459) (2013) 419–425.
- [3] S. Bertolazzi, D. Krasnozhan, A. Kis, Nonvolatile memory cells based on MoS<sub>2</sub>/graphene heterostructures, *ACS Nano* 7 (4) (2013) 3246–3252.
- [4] J.C. Meyer, C.O. Girit, M.F. Crommie, A. Zettl, Hydrocarbon lithography on graphene membranes, *Appl. Phys. Lett.* 92 (2009) 123110–123110–3.
- [5] K.S. Novoselov, A.K. Geim, S.V. Morozov, D. Jiang, Y. Zhang, S.V. Dubonos, I. V. Grigorieva, A.A. Firsov, Electric field effect in atomically thin carbon films, *Science* 306 (2004) 666–669.
- [6] C. Gerbig, A. Sentfleben, S. Morgenstern, C. Sarpe, T. Baumert, Spatio-temporal resolution studies on a highly compact ultrafast electron diffractometer, *New J. Phys.* 17 (4) (2015) 43050.
- [7] G. Sciaini, R.J.D. Miller, Femtosecond electron diffraction heralding the era of atomically resolved dynamics, *Rep. Prog. Phys.* 74 (2011) 96101.
- [8] A.H. Zewail, 4d ultrafast electron diffraction, crystallography, and microscopy, *Annu. Rev. Phys. Chem.* 57 (2006) 65–103.
- [9] C. Kealhofer, S. Lahme, T. Urban, P. Baum, Signal-to-noise in femtosecond electron diffraction, *Ultramicroscopy* 159 (2015) 19–25.
- [10] Lutz Waldecker, Roman Bertoni, Ralph Ernstorfer, Compact femtosecond electron diffractometer with 100 keV electron bunches approaching the single-electron pulse duration limit, *J. Appl. Phys.* 117 (4) (2015) 44903.
- [11] A. Hanisch-Blicharski, A. Janzen, B. Krenzer, S. Wall, F. Klasing, A. Kalus, T. Frigge, M. Kammler, M. Horn-von Hoegen, Ultra-fast electron diffraction at surfaces: from nanoscale heat transport to driven phase transitions, *Ultramicroscopy* 127 (2013) 2–8.
- [12] M. Gulde, S. Schweda, G. Storeck, M. Maiti, H.K. Yu, A.M. Wodtke, S. Schäfer, C. Ropers, Ultrafast low-energy electron diffraction in transmission resolves polymer/graphene superstructure dynamics, *Science* 345 (6193) (2014) 200–204.
- [13] R.P. Chatelain, V.R. Morrison, L.M. Klarenaar, B.J. Siwick, Coherent and incoherent electron-phonon coupling in graphite observed with radio-frequency compressed ultrafast electron diffraction, *Phys. Rev. Lett.* 113 (2014) 235502.
- [14] N. Erasmus, M. Eichberger, K. Haupt, I. Boshoff, G. Kassier, R. Birmurske, H. Berger, J. Demars, H. Schwoerer, Ultrafast dynamics of charge density waves in 4 h(b)-tase2 probed by femtosecond electron diffraction, *Phys. Rev. Lett.* 109 (16) (2012) 55 167402–167402–5.
- [15] K. Hermann, Periodic overlayers and moiré patterns: theoretical studies of geometric properties, *J. Phys. Condens. Matter: Inst. Phys. J.* 24 (31) (2012) 314210.
- [16] J.C. Meyer, A.K. Geim, M.I. Katsnelson, K.S. Novoselov, T.J. Booth, S. Roth, The structure of suspended graphene sheets, *Nature* 446 (2007) 60–63.
- [17] A. Castellanos-Gomez, M. Buscema, R. Molenaar, V. Singh, L. Janssen, H.S.J. van der Zant, G.A. Steele, Deterministic transfer of two-dimensional materials by all-dry viscoelastic stamping, *2D Materials* 1 (1) (2014) 11002.
- [18] R.R. Nair, P. Blake, A.N. Grigorenko, K.S. Novoselov, T.J. Booth, T. Stauber, N.M. R. Peres, A.K. Geim, Fine structure constant defines visual transparency of graphene, *Science* 320 (2008) 1308–1316.
- [19] A. Castellanos-Gomez, R. Roldán, E. Cappelluti, M. Buscema, F. Guinea, H.S. J. van der Zant, G.A. Steele, Local strain engineering in atomically thin MoS<sub>2</sub>, *Nano Lett.* 13 (11) (2013) 5361–5366.
- [20] National Institute of Standards and Technology. (<http://physics.nist.gov/PhysRefData/FFast/html/form.html>). accessed 29-October-2015.